AAS 11-498

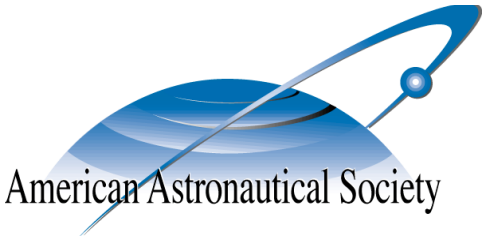

American Institute of
Aeronautics and Astronautics

CIRCULAR ORBIT RADIUS CONTROL USING ELECTROSTATIC ACTUATION FOR 2-CRAFT CONFIGURATIONS

Hanspeter Schaub and Lee E. Z. Jasper

AAS/AIAA Astrodynamics Specialists Conference

Girdwood, Alaska July 31 – August 4, 2011

AAS Publications Office, P.O. Box 28130, San Diego, CA 92198

AAS 11-498

CIRCULAR ORBIT RADIUS CONTROL USING ELECTROSTATIC ACTUATION FOR 2-CRAFT CONFIGURATIONS

Hanspeter Schaub* **and Lee E. Z. Jasper†**

Electrostatic static actuation of free-flying spacecraft is being considered to directly control spacecraft relative motion. This paper investigates the effectiveness of using active electrostatic charging to perform orbit altitude adjustments of a nominally circular orbit. Coulomb forces are employed to gently pull a charged object in the along track direction. In contrast to prior work, this study uses an enhanced electrostatic force model which accounts for the increased capacitance of an object if another charged object is nearby with opposite charge polarity. The pulling configuration is shown to provide larger electrostatic forces over a pushing configuration due to the coupled capacitance modeling. Variational equations are developed to estimate the semi-major axis changes if spherical objects with controlled electrostatic potentials are actuated in the along-track direction. Numerical sweeps are performed to illustrate that kilo-Volt levels of potential are sufficient to achieve kilometer level radius changes per orbit for geosynchronous orbit regimes.

INTRODUCTION

Close proximity spacecraft operations on the order of dozens of meters are challenging endeavors in that frequent orbit corrections are required to compensate for the orbital perturbations, and the close proximity makes the thruster exhaust plume impingement issues more severe. Over the last decade several methods of performing propellantless relative motion control have begun to be explored using electrostatic[1–4] or electro-magnetic forces.[5–8] Lorentz-augmented orbits consider controlling the spacecraft inertial, not relative, motion using a highly charged vehicle flying in the planets magnetic field to create small Lorentz forces.[9–11] All such concepts have the significant advantage that essentially only electrical energy is employed to achieve spacecraft actuation.

For the electrostatic (Coulomb) spacecraft application this has led to a broad set of research investigating virtual Coulomb Structures where natural relative equilibria of the charged relative motion dynamics are explored,[12–16] virtual Coulomb tethers where the electrostatic force replaces a physical between between two end objects,[17–20] or general cluster control algorithms for swarms of charged satellites.[21–25] The Coulomb actuation for space applications is exciting because it can be achieved using only Watt-levels of electrical power for geostationary applications with I_{sp} fuel efficiency values ranging as high as $10^9 - 10^{12}$ seconds.[1,12] Spacecraft charging occurs naturally due to the interaction with the local space environment, and can reach 10's of kilo-Volt during Earth-shaded segments of geosynchronous orbits as demonstrated with the ATS-6 data.[26,27] The Coulomb Formation Flying (CFF) research is investigating charged relative motion subject to actively controlled

*Associate Professor, H. Joseph Smead Fellow, Aerospace Engineering Sciences Department, University of Colorado, Boulder, CO 80309-0431.

†Graduate Research Assistant, Aerospace Engineering Sciences Department, University of Colorado, Boulder, CO 80309-0431.

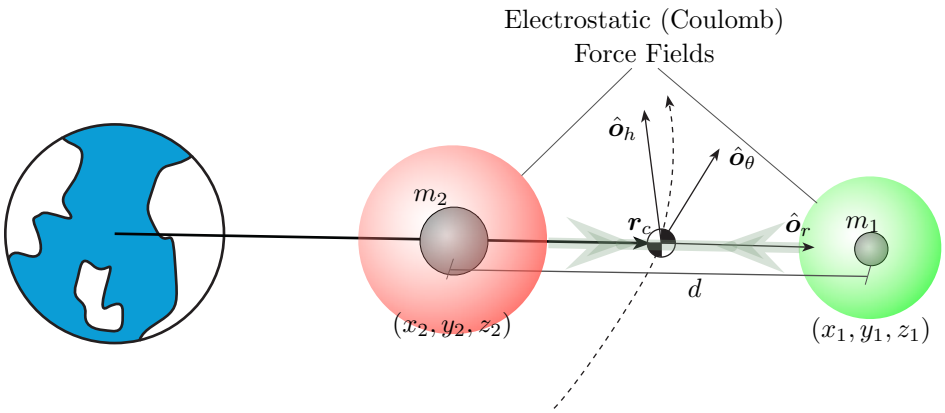

Figure 1. Nadir-Aligned Charge Equilibrium for a Two-Vehicle Configuration

spacecraft potentials on the order of 10's of kilo-Volts. These potential levels have been shown to occur naturally with the right space weather conditions. To maintain a desired spacecraft potential or charge level over time, continuous charge emission is required to shift the natural charge equilibrium to a desired value.[1,12]

This prior CFF research considers the use of electrostatic forces to directly control the relative motion of two or more vehicles. However, an open question that remains is how are orbit correction maneuvers performed if the Coulomb spacecraft cluster elements are not physically interconnected. For example, Natarajan examines the feedback control problem two-craft charged equilibrium configurations in orbit radial alignment as illustrated in Figure 1.[17,20] However, the goal of hybrid charge or thruster control solutions is to stabilize the relative motion about a relative motion equilibrium. The center of mass of such two-craft system is free to drift with orbital perturbations. As with non-fractionated spacecraft, there is a need to periodically adjust the orbit to maintain particular mission sensing requirements. While the electrostatic actuation is achievable with only Watt-levels of electrical power, and essentially no fuel, the resulting forces are still very small, on the order of milli- to micro-Newton level. Thus, any orbit corrections of an electrostatic cluster will require a) that the orbit correction thrust levels are less than the electrostatic force level, or b) that all individual components have thrusters to perform their own inertial thruster. The later case may not be practical for many scenarios. The focus of this paper is to investigate the first scenario (a) where only one component is performing inertial thrusting to change the cluster center of mass motion.

The first application of performing orbit corrections while electrostatically interacting with a secondary spacecraft is discussed by Schaub and Moorer in Reference 28. Here the Geosynchronous Larger Debris Reorbiter (GLiDeR^{TM}) concept is presented where electrostatic forces are employed to tug on large space debris to reorbit it to a disposal orbit. This prior study employs simple point-charge model of the charged bodies. Enhanced electrostatic force modeling is presented in the current study which accounts for position-dependent capacitance models of neighboring charged bodies. Using the spacecraft potential as a fundamental control variable instead of charge as in Reference 28, the amount of charge that is stored on an object is influenced by the presence of additional charged objects. In the present study only circular to circular orbit corrections are considered where the orbit semi-major axis is changed through the application of long-term small inertial thrusting in the along-track direction. Both pushing and pulling along-track aligned configurations are considered and compared. The transitional relative motion dynamics due to the initial thruster engagement

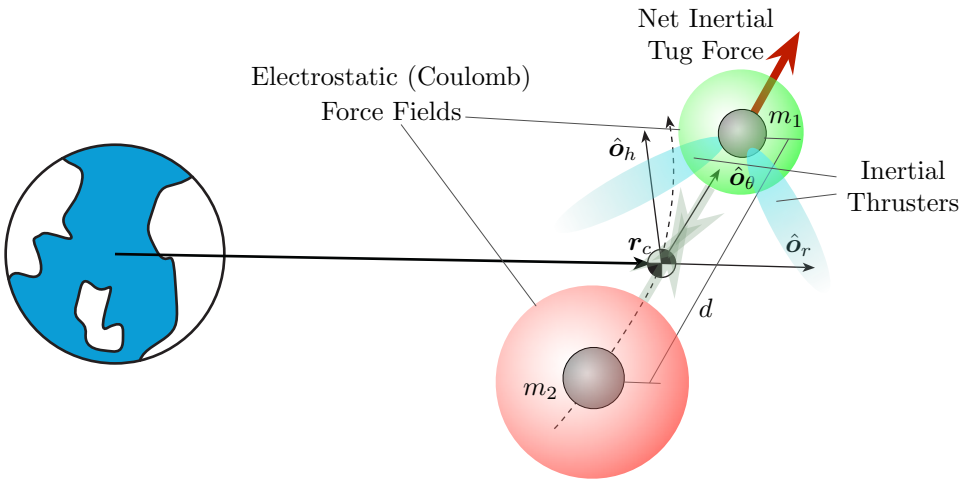

Figure 2. Along-Track Aligned Orbit Correction of a Charged Two-Vehicle Configuration

is beyond the scope of this paper.

In this study the two vehicles are assumed to already be in a nominal along-track configuration as illustrated in Figure 2, and a separation distance feedback control is presented which maintains a nominal separation distance during the orbit correction. The primary interest is the prediction of how well electrostatic forces can be used to move objects with a range of masses and sizes. Numerical sweeps are performed to consider the semi-major axis changing performance of two scenarios. The first scenario considers a fractionated spacecraft concept, similar to the one proposed by the F6 fractionated spacecraft program,[29] where separate spacecraft components contain the specialized inertial thrusting equipment. Here a spherical Coulomb spacecraft is flying in close proximity to a large geostationary satellite whose potential is also controlled to a desired non-zero value. The vehicle with the inertial thrusting capability is acting as a space tug for the second craft. Of interest are the following issues: can the relatively small electrostatic forces be employed to move or tug large GEO satellites to a new orbit radius, and what time would be required for such low-thrust maneuvers. The second scenario considered in this paper assumes the secondary vehicle (spacecraft without inertial thrusting duties) is a smaller free-flying sensor that is electrostatically tethered to the large mothercraft. The primary craft will be able to contain much more charge than the smaller secondary sensor vehicle. Of interest is how the resulting electrostatic force impacts any semi-major axis correction maneuvers.

POTENTIAL BASED ELECTROSTATIC TUG FORCE EVALUATION

Position Dependent Capacitance

The electrostatic force between two point charges q_1 and q_2 separated by a distance d in a vacuum is given by

$$F_c = k_c \frac{q_1 q_2}{d^2} \tag{1}$$

where $k_c = 8.99 \cdot 10^9$ Nm^2/C^2 is the Coulomb constant. The vast majority of CFF research considers the dynamics and control of point charges. Even if the charged cluster elements are controlled via

their potential as in Reference 12, then the isolated sphere voltage to charge relationship

$$V = k_c \frac{q}{r} \tag{2}$$

is employed with r being the sphere radius. This charge to voltage relationship is only valid for a single sphere, and not for a cluster of neighoring spheres. As experimentally verified for the CFF application by Seubert in Reference 30, the presence of another object with non-zero potential will fundamentally change the charge to voltage relationship. With Coulomb spacecraft the natural charge equilibrium with the spacecraft is disturbed through continuous charge emission as demonstrated in the SCATHA and ATS missions in the 1970's,[31–33] or in the current European CLUSTER mission.[34,35] The vehicle's potential is controlled through the potential of the electron or ion emission. In this study we are considering a scenario where the vehicle's absolute potential is held fixed through active charging, and we wish to determine the strength of the resulting electrostatic interaction between two spheres of radii r_1 and r_2 respectively as illustrated in Figure 3.

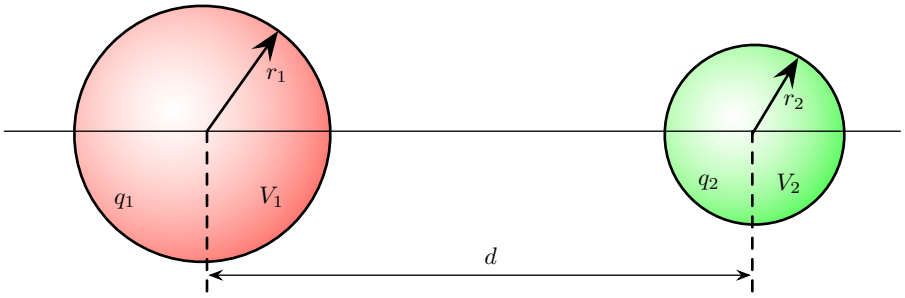

Figure 3. Illustration of Two Close Proximity Charged Spheres

Assume the two conducting spheres have each a potential V_1 and V_2. The potential on sphere 1 is computed as the sum of the self-capacitance relationship in Eq. (2) and the potential due to the second body of charge q_2 as:[36,37]

$$V_1 = k_c \frac{q_1}{r_1} + k_c \frac{q_2}{d} \tag{3}$$

Equivalently, the absolute potential on the surface of the conducting sphere 2 is expressed as the sum:

$$V_2 = k_c \frac{q_2}{r_2} + k_c \frac{q_1}{d} \tag{4}$$

Note that the potentials in this paper are all assumed to be taken relative to a zero potential at infinity. Even with spheres held at fixed potentials, the charge distribution can be non-homogenous if the two spheres are very close to each other.[38] However, this induced charge effect is negligible if the separation distance is more than 3-4 craft radii as is assumed in this study.

Solving Eqs. (3) and (4) for the charges yields:[36,37]

$$\begin{bmatrix} q_1 \\ q_2 \end{bmatrix} = \underbrace{\frac{d}{k_c(d^2 - r_1 r_2)} \begin{bmatrix} r_1 d & -r_1 r_2 \\ -r_1 r_2 & r_2 d \end{bmatrix}}_{[C(d)]} \begin{bmatrix} V_1 \\ V_2 \end{bmatrix} \tag{5}$$

The 2×2 matrix $[C(d)]$ is the capacitance matrix for this two-sphere system which is a function of the separation distances. Note that depending on the sign of the other bodies potentials, the amount of charge stored on each sphere can be either increased or decreased in contrast to the isolated sphere charge/voltage relationship in Eq. (2)

Substituting the charges q_1 and q_2 in Eq. (5) into the electrostatic force expression in Eq. (1) yields:

$$F_c = \frac{r_1 r_2 (r_1 V_1 - d V_2)(r_2 V_2 - d V_1)}{k_c (d^2 - r_1 r_2)^2} \tag{6}$$

This position dependence capacitance relationship has been experimentally verified using the one-dimensional electrostatic charged relative motion test bed in Reference 30, as well as numerically verified with finite element based electrostatic field solvers such as Maxwell3D.

Pulling and Pushing Configuration Considerations

To perform low-thrust Semi-Major Axis (SMA) corrections, the most efficient thrusting solution is in the current along-track direction.[39] For a cluster of only 2 Coulomb spacecraft, this yields two possible scenarios to perform the SMA changes where the thrusting vehicle is either in the lead tugging, or in the rear pushing the second charged vehicle. The pulling or tugging configuration requires an attractive electrostatic force between the two bodies, and thus the potentials must satisfy the condition $V_1 V_2 < 0$.

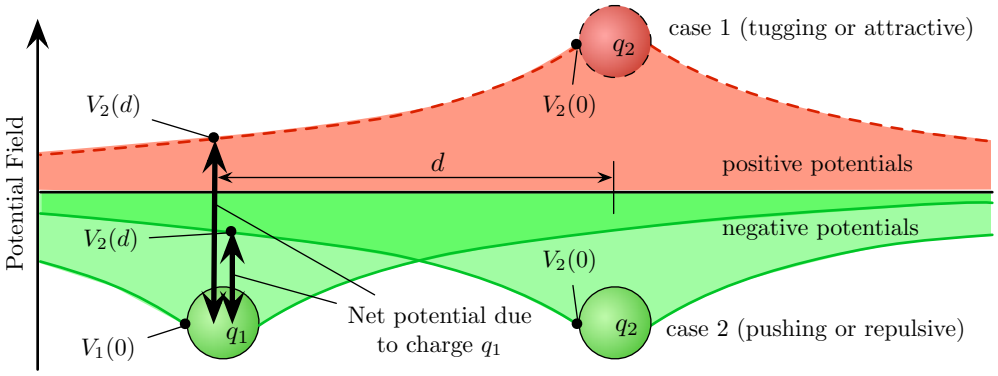

Figure 4. Illustration of Neighboring Potential Impact on local Capacitance

Studying the electrostatic force expression in Eq. (6), it is evident that having potentials with opposite signs causes an increase in the electrostatic force. The reason for this force increase is observed in the studying the capacitance matrix in Eq. (5). If the potentials have opposite signs, then both V_1 and V_2 will contribute to increasing the magnitudes of q_1 and q_2. Thus, if the potentials V_1 and V_2 are held fixed, and the separation distance is changed, then the charges q_i will vary. This process is visualized in Figure 4 showing an electrostatic attractive (case 1) and repulsive (case 2) scenario. While sphere 1 is holding a fixed potential $V_1(0)$ on its surface, the amount of charge stored on the sphere to achieve this potential is dependent on the potential fields of neighboring objects. For example, assume that the conducting sphere 1 has no potential control active. Because of the presence of a second object with charge q_2, sphere 1 will assume the potential $V_2(d)$ that the second sphere yields at a separation distance d. Consider case 1 where $V_1 V_2 < 1$. Without loss

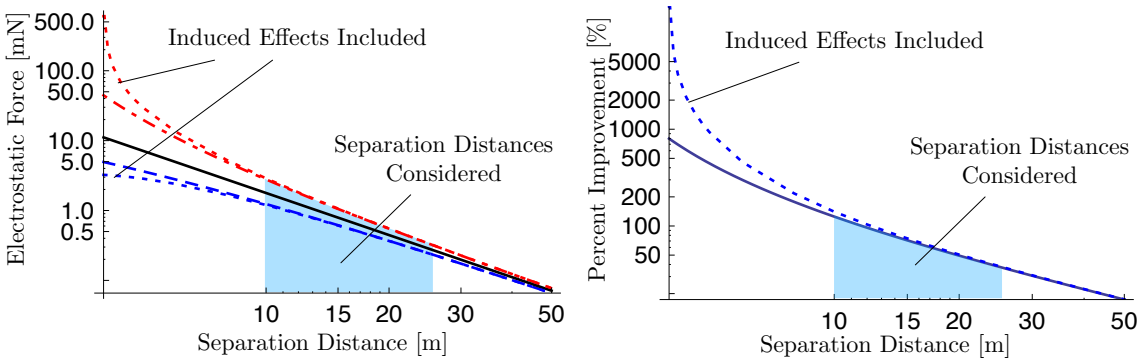

(a) Force Magnitude Comparison

(b) Ratio of Attractive versus Repulsive Forces

Figure 5. Electrostatic Force Illustration for two 2-meter radius spheres at 20kV. Cases shown include repulsive spheres (– – –), attractive spheres (– · – · –), cases with induced charge effects included (· · ·), and the reference case assuming two isolated spheres (——)

of generality, assume V_2 is positive. Here body 1 must accumulate negative charge just to bring its potential down to zero. To achieve the desired $V_1(0) < 0$ value, additional negative charge is required. In contrast, with case 2 both spheres have the same charge polarity. Here the first sphere will already have a negative potential without any additional charge accumulation. Thus, less negative charge is required to reach the desired $V_1(0)$ surface potential.

The impact of this position dependent capacitance on the resulting electrostatic force magnitude is illustrated in Figure 5. Three primary cases are considered, each with two spheres with 2 meter radii and 20kV potential magnitudes. The solid line computes the electrostatic forces assuming each sphere is isolated with the charge computed using Eq. (2). The dashed-dotted line considers an electrostatic attractive force scenario where $V_1 V_2 < 0$ and uses Eq. (5) to evaluate the charges. The dashed line illustrates the force magnitude for a repulsive scenario with $V_1 V_2 > 0$ also evaluated using Eq. (5). The smallest feasible separation distance in this scenario is 4 meters where the sphere surfaces would be touching. At this point the attractive force scenario yields a 4 times larger electrostatic force for the same potential in comparison to the isolated sphere model. The repulsive scenario yields a force that is about half. Naturally electrostatic reorbiting will not occur with the object almost touching each other. Instead, CFF considers center-to-center separation distances of 10-25 meters. As illustrated in Figure 5(b), for separation distance ranging 10-25 meters, the attractive electrostatic force can be 50-100% larger compared the repulsive electrostatic force magnitude for equivalent potential magnitudes. Thus, from an electrostatic force evaluation perspective, the tugging scenario with attractive electrostatic forces yields significant performance improvements for performing electrostatic orbit corrections.

Figure 5 also shows the expected electrostatic force between two spheres if induced charge effects are included using the iterative solution provided by Soules in Reference 38. Here the non-homogenous charge distribution on two conductive surfaces causes an increase in the attractive force. This results in a strengthening of the electrostatic attraction over very short distance (less then 3-4 craft radii), and additional weakening of the repulsive force. This further favors the pulling orbit correction configuration.

Besides the electrostatic force argument for a given voltage level, another argument favoring the

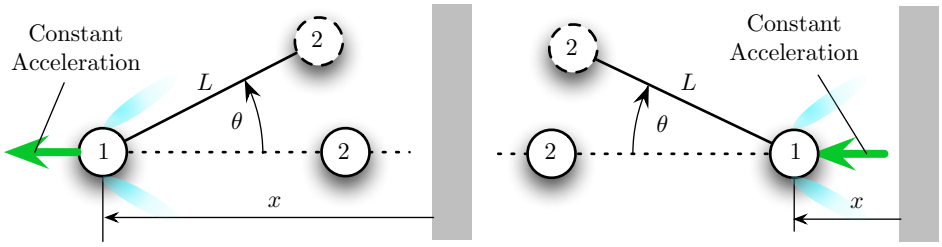

(a) Pulling Configuration (b) Pushing Configuration

Figure 6. Dynamic Illustration of a Pushed and Pulled Fixed Length Pendulum Configuration Subject to a Constant Acceleration on Object 1.

pulling configuration for orbit corrections is the resulting relative dynamics. Even if the separation distance between the satellite is being held fixed with a feedback control strategy, the relative orientation of the two satellites is open-loop unstable. The two configurations considered are illustrated in Figure 6. If we consider $\ddot{x} > 0$ a constant acceleration, and $\dot{x}(t) > 0$, then the linear angular departure motion θ differential equations are either:

$$L\ddot{\theta} + \dot{x}\dot{\theta} + \ddot{x}\theta = 0 \qquad \text{(pulling)} \tag{7a}$$

$$L\ddot{\theta} - \dot{x}\dot{\theta} - \ddot{x}\theta = 0 \qquad \text{(pushing)} \tag{7b}$$

The positive pushing acceleration causes a negative stiffness, and thus unstable relative orientation oscillations. In contrast, the pulling configuration leads to stable oscillations in this simple dynamic illustration example. For the electrostatic orbit correction application, it will be significantly simpler to control the relative motion with the second object if the thrusting object is in the lead pulling the other. The pulling configuration will require that the lead's exhaust plume does not impinge on the second object. This can be achieved with angled or boom-displaced thrusters which direct the exhaust plume into free space.

Space Weather Impact

These charge to voltage relationships assume that the space weather impact is negligible. As discussed by Denton et. al. in Reference 40, the nominal space weather can vary across the geosynchronous orbit region as different local time locations are considered, as well as due to solar disturbances to Earth magnetic field expressed through the K_p index. For GEO environments the Debye length λ_D is given by

$$\lambda_D = \sqrt{\frac{\epsilon_0 T_e}{eN}} \tag{8}$$

where the electron temperature T_e is given in units of eV, N is the charged particle density in units of m^{-3}, e is the electron charge and ϵ_0 is the permittivity of free space. If the spacecraft potential V is small compared to the plasma temperature T_e and $eV \leq kT_e$ is satisfied, then the approximate potential relationship about a finite sphere with a surface potential V_s and radius r in this plasma is

$$V(d) = V_s \frac{r}{d} e^{-d/\lambda_D} \tag{9}$$

Reference 40 studies the nominal plasma temperatures and densities for a 10 year period. The results indicate that the minimum Debye lengths across a GEO orbit range between 180–200 meters,

depending on the solar activity and the local time. This charge shielding distance is much larger than the small separation distances of 10-50 meters considered in this study. Further, because relatively large potentials are being considered relative to the GEO plasma energy levels, the small relative potential approximation of Eq. (9) only yields conservative worst-case estimates of the amount of charge shielding that would be experienced. The large potentials result in a weakening of the charge shielding, as discussed in Reference 41, and much larger effective Debye lengths. Thus, the omission of the space weather influence on performing electrostatic orbit corrections is justifiable for a first order performance study. Future work could consider space weather extremes that might be encountered, and how this impacts the non-trivial electrostatic force and vehicle capacitance relationship.

ELECTROSTATIC SEMI-MAJOR AXIS CHANGES

Orbital variational equations are used next to obtain analytical predictions of the amount of semi-major axis changes Δa that are feasible for ranges of spacecraft potentials, dimensions, and mass. Let a_r and a_θ be the orbit radial and along-track disturbance accelerations. Gauss' variational equation for the SMA a is[39,42]

$$\frac{\mathrm{d}a}{\mathrm{d}t} = \frac{2a^2}{h}\left(e\sin f a_r + \frac{p}{r}a_\theta\right) \tag{10}$$

where h is the orbit angular momentum, p is the semi-latus rectum, e is the eccentricity, f is the true anomaly, and r is the current orbit radius. For this study the Coulomb spacecraft cluster is assumed to have a near zero eccentricity with $e \to 0$, $r \to a$ and $p \to a$. While the orbit correction is accomplished through a spiraling trajectory, the path can be locally approximated as a circle. For a nearly-circular orbit with a vanishingly small eccentricity, the momentum is approximated through

$$h = \sqrt{\mu p} = r^2\dot{f} \approx a^2 n \tag{11}$$

where μ is the gravitational constant, and n is the mean orbit rate. The SMA differential equation in Eq. (10) reduces to

$$\frac{\mathrm{d}a}{\mathrm{d}t} = \frac{2a_\theta}{n} \tag{12}$$

Let m_1 be the mass of the object performing the inertial thrusting, and m_2 be the object that is electrostatically towed to a new orbit. The along-track acceleration of m_2 is given by

$$a_\theta = \frac{|F_c|}{m_2} \tag{13}$$

where the electrostatic force acting on m_2 is determined through Eq. (6). The absolute value operator is employed with F_c to account that a_θ is positive for both the pulling and pushing configurations considered. Thus, while the pulling configuration is preferred, the following development holds for both cases.

Let $P = 2\pi/n$ be the orbit period, then the SMA change per orbit due to a constant along-track acceleration a_θ is approximated through

$$\Delta a \approx \frac{\mathrm{d}a}{\mathrm{d}t}\cdot P = \frac{4\pi}{n^2}a_\theta \tag{14}$$

Substituting Eq. (6) and (13) into Eq. (14) yields an estimate of the SMA change that can be produced over one orbit revolution:

$$\Delta a \approx \frac{4\pi}{n^2} \frac{r_1 r_2 (r_1 V_1 - d V_2)(r_2 V_2 - d V_1)}{k_c m_2 (d^2 - r_1 r_2)^2} \tag{15}$$

In contrast to the SMA change prediction provided in Reference 28, the Δa per orbit expression in Eq. (15) explicitly accounts for the position dependent capacitance results from neighboring charged objects. The SMA change performance is still inversely proportional to the mass m_2 that is being towed to a new orbit. However, in contrast to earlier work using simplifying isolated sphere charge to voltage relationships, the SMA change performance is now a complex relationship between separation distance d and effective spherical radii r_i of either object. The following section employs numerical sweeps to illustrate the expected performance levels to apply orbit corrections to both large and small geosynchronous objects.

NUMERICAL SMA PERFORMANCE STUDY

Case 1: Towing Large Geostationary Objects

First, let us consider the case where the second object is being electrostatically towed to a new SMA. In this scenario, the two-body system could be considered a fractionated spacecraft concept where the a free-flying element contains the inertial thrusters to perform the orbit corrections, while the second object contains the science or communication instruments of the geostationary satellite.

In this scenario the tugging vehicle 1 is assumed to have a spherical shape of radius r_1, while the second object could be a regular satellite with a general three-dimensional shape. However, the Eq. (15) assumes both objects are spheres. The question arises regarding how a general shape can be represented through an effective sphere. Reference 43 provides an extensive study on how well three-dimensional shapes can be represented through effective spheres. As with gravitational fields about three-dimensional shapes, the larger the separation distance is, the more the field approaches that of a sphere. Reference 43 demonstrates that with even with solar panels expanding 4-7 meters from the spacecraft center, for separation distances larger than 15 meters the 1$^{\text{st}}$-order effective sphere model deviates from the exact 3D electrostatic models by only 10-15% at worst. For cylindrical shapes, such as used with dual-spinner satellites, the deviations over these separation distances is 5% or less.

The 1$^{\text{st}}$-order effective sphere model requires extensive finite element based numerical modeling of the true electrostatic field about a general shape, and then fitting the effective radius to this data. In this study the goal is to obtain approximate SMA performance measures for a range of bodies. Instead of using the 1$^{\text{st}}$-order effective sphere model, this study employs the 0$^{\text{th}}$-order effective sphere model discussed in Reference 43. Here the rough dimensional of the spacecraft are used to estimate the total outer surface area, and then this area is matched to a sphere to yield an equivalent sphere radius. This simpler and faster method yields representative craft radii which can differ by about 10% from the more complex 1$^{\text{st}}$-order method.

Next, to use Eq. (15) to predict SMA changes, it is important that a realistic mass to size relationship is used. For example, a more massive satellite also tends to have a larger size, and thus a larger capacitance. As a result, it is not readily apparent that a larger satellite will result in a lower SMA change performance for a given voltage level.

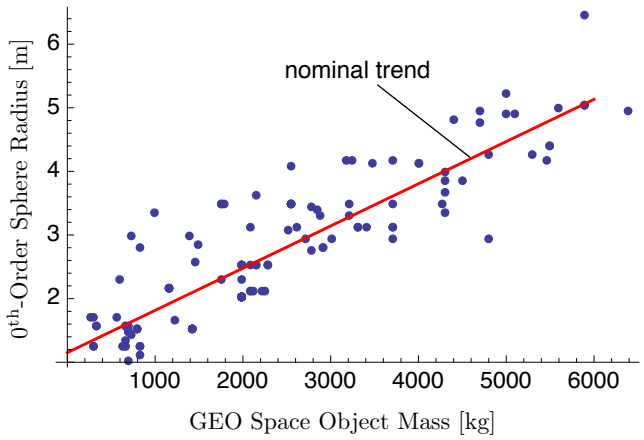

Figure 7. Illustration of the nominal size to mass trend of Geosynchronous RSOs

Using a public NASA web site* discussing geostationary satellite data, the approximate mass and satellite dimensions were obtained. Figure 7 illustrates the resulting mass to 0^{th}-order effective radius for a range of GEO Resident Space Objects (RSO). This data yields a mean mass to radius relationship of

$$r_2(m_2) = 1.152\text{m} + 0.00066350\frac{\text{m}}{\text{kg}}m_2 \tag{16}$$

where r_2 is in units of meters, and m_2 is in units of kilograms. Please note that this relationship of the NASA site provides the launch masses of each satellite. Thus, Eq. (16) illustrates the worst case mass to area ratio you could have. For many older geostationary satellite designs, the fuel stored for orbit corrections is a significant fraction of the total mass. Thus, if a satellite is moved which has expelled its fuel, its mass could be considerably smaller while maintaining the same surface area (capacitance).

SMA Changes With Initial Launch Mass: First, let us consider what SMA changes are feasible per geosynchronous orbit (24 hours) using the Δa approximation in Eq. (15) and the GEO RSO mean mass to radius relationship in Eq. (16). The Coulomb craft with inertial thrusters is ahead of the towed Coulomb vehicle in a pulling configuration.

Figure 8 sweeps the towed mass from 500-5000kg, and the voltages from 0-40kV. This study assumes $V_1 = -V_2$. Four scenarios are shown where with the center-to-center separation distances 25, 20, 15, and 10 meters. Given the larger outer dimensions of many GEO satellites, separation distances shorter than 10 meters result in significant collision risks. The Coulomb vehicle with inertial thruster is assumed to have a radius of 3 meters for all these numerical sweeps.

The ATS-6 mission has shown that natural charging during solar storm activities can reach 18kV. Thus, achieving potential levels of 20kV and larger are feasible. Furthger, if the towed object has a mass of 1000kg, a separation distance of 20 meters, then a 20kV potential would result in SMA changes of about 2 km/day. A 10km correction could be accomplished using a low-thrust spiraling trajectory over only 5 days. If a larger object of 2000kg mass is considered, the SMA changes reduce to about 1.5 km/day. Note that the SMA change performance does not scale with the mass of the towed object because larger objects also act as larger capacitors.

*http://nssdc.gsfc.nasa.gov/nmc/SpacecraftQuery.jsp

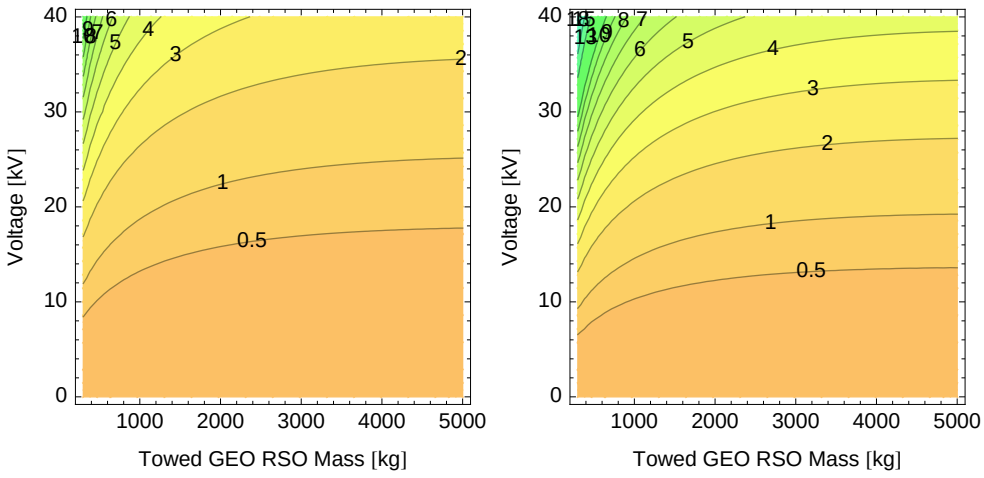

(a) Separation Distance of $L = 25$ meters

(b) Separation Distance of $L = 20$ meters

(c) Separation Distance of $L = 15$ meters

(d) Separation Distance of $L = 10$ meters

Figure 8. Kilometer SMA changes per orbit period for a range of towed object masses, voltages, and separation distances. These results assume a launch mass to area relationship of GEO RSOs, and a tow-vehicle radius r_1 of 3 meters.

Shorter separation distances have a strong impact on the SMA change performance due to the near-inverse-square relationship between the electrostatic force and separation distance. At 15 meters separation, the 2000kg object results in about 3 km/day SMA changes. Further, if even shorter separation distances are considered, such as 10 meters in Figure 8(d), the performance curve becomes flat, and even reverses direction, indicating that is it possible for more massive object to yield higher SMA change performances.

SMA Changes With 60% Launch Mass: Next, let us consider a mass-to-radius relationship of the towed vehicle which assumes the the current mass is 60% of the initial launch mass. This scenario assumes that a large amount of fuel has been used by the towed vehicle. For electrostatic orbit corrections, this increases the magnitudes of the orbit corrections as the towed vehicle retains the same capacitance, but now has less mass.

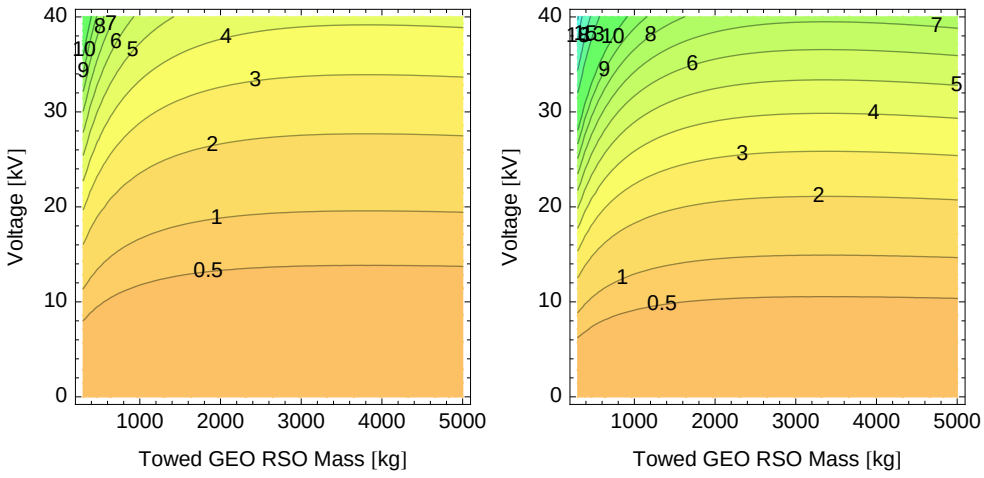

(a) Separation Distance of L = 25 meters

(b) Separation Distance of L = 20 meters

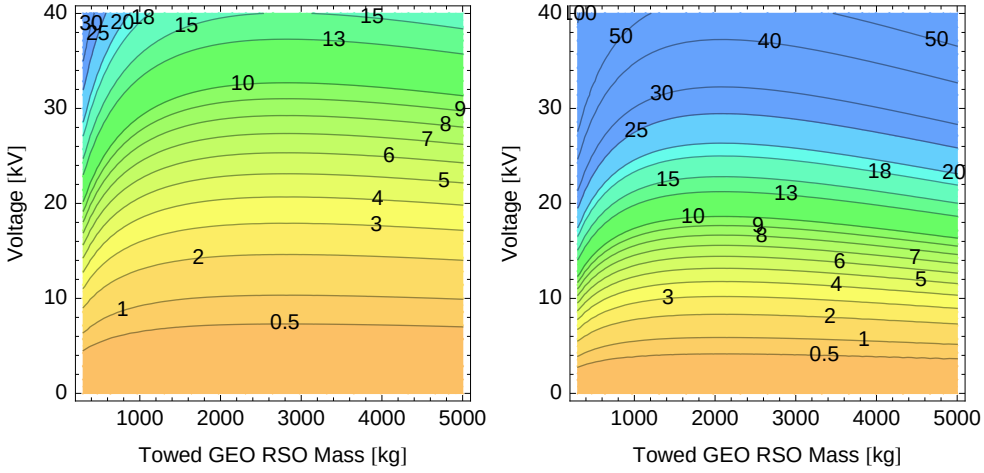

(c) Separation Distance of L = 15 meters

(d) Separation Distance of L = 10 meters

Figure 9. Kilometer SMA changes per orbit period for a range of towed object masses, voltages, and separation distances. These results assume a GEO RSOs mass-to-area relationship with 60% of launch mass, and a tow-vehicle radius r_1 of 3 meters.

The numerical sweeps of Figure 8 are repeated in Figure 9 with this new mass to radius relationship. The SMA change performance for the 2000kg case with 20kV increases from 1.5 km/day to about 2km/day for the 20 meter separation distance scenario. Further, note that with this small mass to radius ratio, the contour lines in Figure 9 are flatter than with the larger mass, and even reverse the trend at smaller masses. This illustrates that electrostatic orbit correction are feasible not only with the smaller GEO satellites, but also with the larger ones. Larger satellites can become easier to reorbit with particular mass to radius ratios.

Let us consider this reverse of SMA change effort in more detail. Assuming a linear radius to mass relationship of the towed vehicle

$$r_2(m_2) = a_0 + a_1 m_2 \tag{17}$$

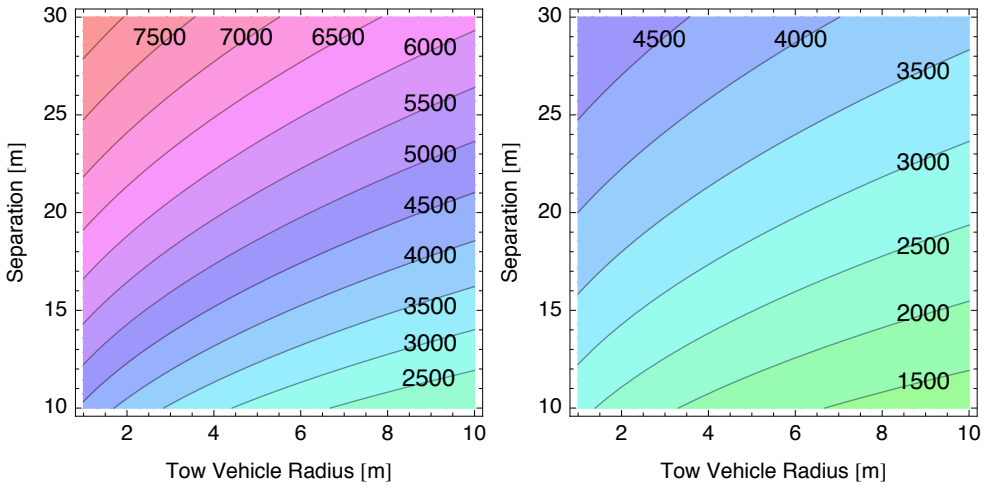

(a) GEO Object Launch Mass Case (b) 60% of GEO Object Launch Mass Case

Figure 10. Critical mass study illustrating from what mass (units of kg) onward the electrostatic orbit correction becomes easier due to the increase object capacitance.

the inflection points of the SMA changes Δa in Eq. (15) with respect to m_2 are of interest. Making the assumption $V_1 = -V_2$, then the SMA correction simplifies to

$$\Delta a \approx \frac{4\pi}{n^2} \frac{r_1 r_2(m_2) V_1^2 (r_1 + d)(r_2(m_2) + d)}{k_c m_2 (d^2 - r_1 r_2)^2} \tag{18}$$

The m_2 inflection points are determined by solving

$$\frac{\partial(\Delta a)}{\partial m_2} = 0 \tag{19}$$

With the potential constraint $V_1 = -V_2$, then the resulting critical masses that satisfy Eq. (19) do not depend on the vehicle potentials.

Figure 10 illustrates the critical towed vehicle masses m_2 for both launch mass and 60% launch mass cases. The center-to-center separation distances are swept from 10-30 meters, and 1-10 meter tug vehicle radii are considered. With the full launch mass, a 3 meter radius tug vehicle with a 20 meter separation distance has a critical tow mass of m_2 = 6000 kg. This means for vehicles more massive than this critical mass, larger changes in the SMA are feasible due to the dominating capacitance impact. If a smaller mass-to-radius relationship of having 60% of the initial launch mass, the same 3 meter tug at 20 meters separation as a lower critical tow mass m_2 of about 3500kg. Further, Figure 10 illustrates the trend that large tug radii will result in lower critical tow masses.

Case 2: Towing a Small Free-Flying Sensor Object

The prior section considered the scenario where a large Coulomb tug is pulling on a large geostationary satellite. Next, the setup is considered where a large GEO mothercraft has a smaller daughter vehicle deployed. The separation distance between the two is controlled through electrostatic forces. The daughter vehicle could be flying 10-20 meters from the mothercraft to provide local situational awareness about the mothercraft, or provide images to inspect the exterior hull for damage due to space debris or micro-meteorites.

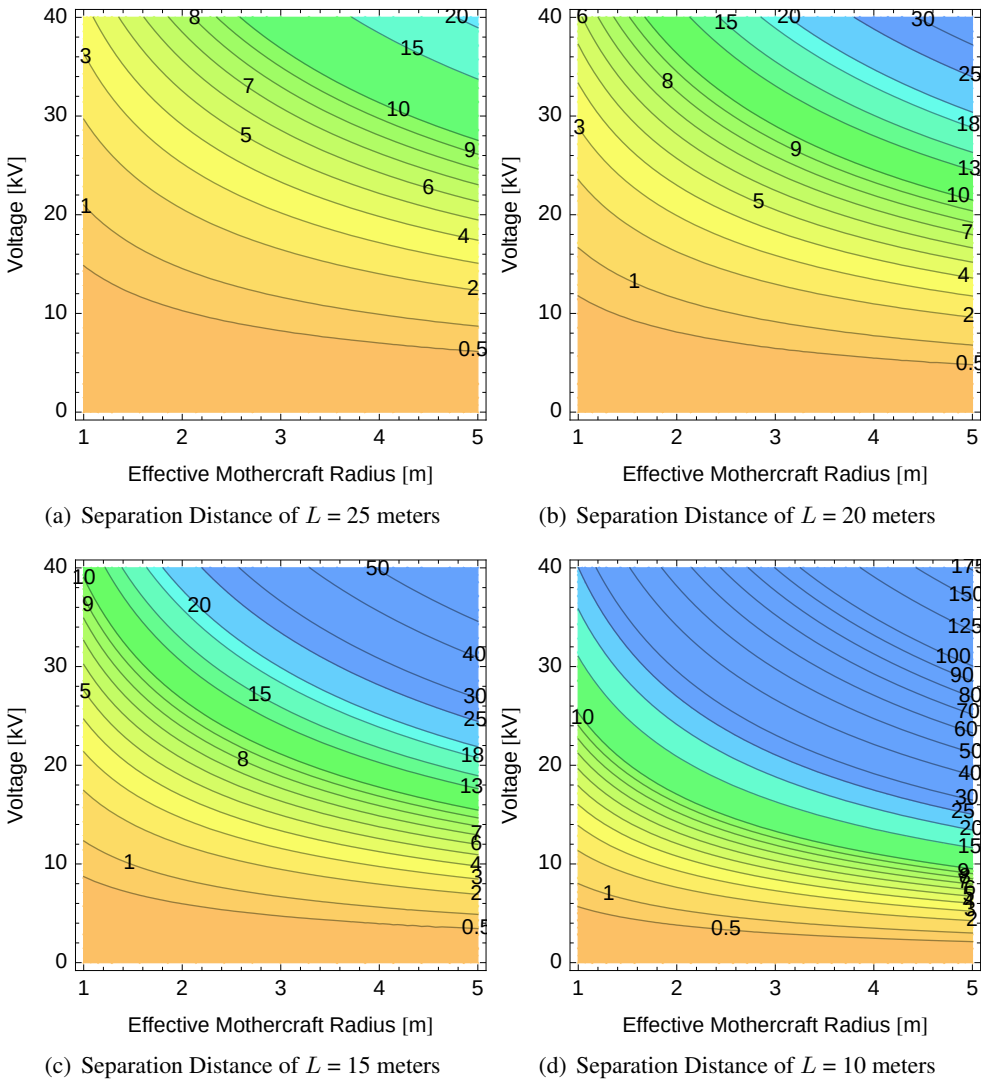

(a) Separation Distance of L = 25 meters

(b) Separation Distance of L = 20 meters

(c) Separation Distance of L = 15 meters

(d) Separation Distance of L = 10 meters

Figure 11. Mother-daughter SMA changes (in kilometers) per orbit period for a range of tow vehicle radii and voltages. The smaller daughter vehicle has a mass of 100kg and radius of 0.5meters.

At first glance it might seem that this is a much easier scenario to perform orbit corrections, as the large mothercraft is towing a much lighter secondary vehicle. However, due to the smaller size of the daughter vehicle, it will also provide a smaller charge capacitance. Figure 11 illustrates the expected SMA changes per orbit (day) assuming the daughter vehicle is a small spherical 100kg vehicle with 0.5 meter radius. Assuming a 20 meter separation distance, an effective mothercraft radius of 3 meters, and $V_1 = -V_2$ = 20 kV, the expected SMA changes are about 4.5 km/orbit. In contrast, the SMA performance in Figure 9(b) shows a performance of about 2-3 km/orbit for masses 1000-5000kg. Thus, the mother-daugher vehicle scenario reinforces the conclusion that lighter or heavier objects are not necessarily easier or more challenging to reorbit electrostatically. A careful study must be performed taking the actual mass to size relationship into account.

CONCLUSION

Coulomb forces have been considered for relative motion control for several years. This paper discusses how to perform simple semi-major axis correction maneuver while two free-flying spacecraft are electrostatically tethered to each other. The charge is studied using the absolute potential of each vehicle. Pulling configurations with attractive electrostatic forces are found to provide larger actuation than pushing configurations with repulsive electrostatic forces. The semi-major axis changes per orbit are analytically predicted using Gauss' variational equations. Numerical performance sweeps illustrate that even large spacecraft can be electrostatically reorbited. In fact, assuming a linear mass to radius relationship, for every separation distance and vehicle potential consideration there is a critical mass beyond which performing orbit corrections at a given potential actually becomes easier again. Further, a mother- and daughter-vehicle case is considered where the daughter vehicle is small and light. While this configuration produces larger semi-major axis changes per orbit, the increase in performance is only marginal compared to the larger object towing case due to the significantly decreased capacitance of the smaller vehicle.

ACKNOWLEDGMENT

We would like to thank the Dr. Daniel Moorer and the Wacari Group for their support of this research, and feedback on the viability of this concept. We also thank Dr. Daniel Baker for helpful discussions on GEO space weather variability.

REFERENCES

[1] J. H. Cover, W. Knauer, and H. A. Maurer, "Lightweight Reflecting Structures Utilizing Electrostatic Inflation," US Patent 3,546,706, October 1966.

[2] H. Schaub, G. G. Parker, and L. B. King, "Challenges and Prospect of Coulomb Formations," *Journal of the Astronautical Sciences*, Vol. 52, Jan.–June 2004, pp. 169–193.

[3] L. B. King, G. G. Parker, S. Deshmukh, and J.-H. Chong, "Study of Interspacecraft Coulomb Forces and Implications for Formation Flying," *AIAA Journal of Propulsion and Power*, Vol. 19, May–June 2003, pp. 497–505.

[4] L. Pettazzi, H. Krüger, S. Theil, and D. Izzo, "Electrostatic Forces for Satellite Swarm Navigation and Reconfiguration," *2^{nd} ACT Workshop on Innovative Concepts*, ESTEC, 2008.

[5] E. M. C. Kong and D. W. Kwon, "Electromagnetic Formation Flight For Multisatellite Arrays," *Journal of Spacecraft and Rockets*, Vol. 41, July–Aug. 2004.

[6] D. W. Miller, , R. J. Sedwick, E. M. C. Kong, and S. Schweighart, "Electromagnetic Formation Flight for Sparse Aperture Telescopes," *IEEE Aerospace Conference Proceedings – Volume 2*, Big Sky, Montana, March 9–16 2002.

[7] U. Ashun, "Dynamics and Control of Electromagnetic Satellite Formations in Low Earth Orbits," *AIAA Guidance, Navigation and Control Conference*, Keystone, CO, Aug. 21–24 2006. Paper No. AIAA 2006-6590.

[8] D. D. Villani and P. B. Landecker, "Magnetic systems and methods for realizing spacecraft maneuvers," US Patent 6,089,510, July 18 2000.

[9] H. Yamakawa, M. Bando, K. Yano, and S. Tsujii, "Spacecraft Relative Dynamics under the Influence of Geomagnetic Lorentz Force," *AIAA Guidance, Navigation and Control Conference*, Toronto, Canada, Aug. 2–5 2010. Paper No. AIAA 2010-8128.

[10] M. A. Peck, B. Streetman, C. M. Saaj, and V. Lappas, "Spacecraft Formation Flying using Lorentz Forces," *Journal of British Interplanetary Society*, Vol. 60, July 2007, pp. 263–267.

[11] M. A. Peck, "Prospects and Challenges for Lorentz-Augmented Orbits," *AIAA Guidance, Navigation and Control Conference*, San Francisco, CA, August 15–18 2005. Paper No. AIAA 2005-5995.

[12] L. B. King, G. G. Parker, S. Deshmukh, and J.-H. Chong, "Spacecraft Formation-Flying using Inter-Vehicle Coulomb Forces," tech. rep., NASA/NIAC, January 2002. `http://www.niac.usra.edu`.

[13] J. Berryman and H. Schaub, "Static Equilibrium Configurations in GEO Coulomb Spacecraft Formations," *Advances in Astronautical Sciences*, Vol. 120, American Astronautical Society, 2005, pp. 51–68. Paper No. AAS 05–104.

[14] H. Schaub, C. Hall, and J. Berryman, "Necessary Conditions for Circularly-Restricted Static Coulomb Formations," *Journal of the Astronautical Sciences*, Vol. 54, July-Dec. 2006, pp. 525–541.

[15] J. Berryman and H. Schaub, "Analytical Charge Analysis for 2- and 3-Craft Coulomb Formations," *AIAA Journal of Guidance, Control, and Dynamics*, Vol. 30, Nov.–Dec. 2007, pp. 1701–1710.

[16] H. Vasavada and H. Schaub, "Analytic Solutions for Equal Mass Four-Craft Static Coulomb Formation," *Journal of the Astronautical Sciences*, Vol. 56, Jan. – March 2008, pp. 17–40.

[17] A. Natarajan, H. Schaub, and G. G. Parker, "Reconfiguration of a Nadir-Pointing 2-Craft Coulomb Tether," *Journal of British Interplanetary Society*, Vol. 60, June 2007, pp. 209–218.

[18] A. Natarajan and H. Schaub, "Orbit-Nadir Aligned Coulomb Tether Reconfiguration Analysis," *Journal of the Astronautical Sciences*, Vol. 56, Oct. – Dec. 2008, pp. 573–592.

[19] A. Natarajan and H. Schaub, "Linear Dynamics and Stability Analysis of a Coulomb Tether Formation," *AIAA Journal of Guidance, Control, and Dynamics*, Vol. 29, July–Aug. 2006, pp. 831–839.

[20] A. Natarajan and H. Schaub, "Hybrid Control of Orbit Normal and Along-Track Two-Craft Coulomb Tethers," *Aerospace Science and Technology*, Vol. 13, June–July 2009, pp. 183–191.

[21] S. Wang and H. Schaub, "Switched Lyapunov Function Based Coulomb Control of a Triangular 3-Vehicle Cluster," *Advances in Astronautical Sciences*, Vol. 135, American Astronautical Society, 2009, pp. 1477–1496. Paper AAS 09–391.

[22] S. Wang and H. Schaub, "Nonlinear Charge Control for a Collinear Fixed Shape Three-Craft Equilibrium," *AIAA Journal of Guidance, Control, and Dynamics*, Vol. 34, Mar.–Apr. 2011, pp. 359–366, doi: 10.2514/1.52117.

[23] S. Wang and H. Schaub, "1-D Constrained Coulomb Structure Stabilization With Charge Saturation," *Advances in Astronautical Sciences*, Vol. 129, Mackinac Island, MI, American Astronautical Society, 2007, pp. 257–274. Paper AAS 07–267.

[24] C. Saaj, V. J. Lappas, H. Schaub, and D. Izzo, "Hybrid propulsion system for formation flying using electrostatic forces," *Aerospace Science and Technology*, Vol. 14, No. 5, 2010, pp. 348 – 355, DOI: 10.1016/j.ast.2010.02.009.

[25] L. Pettazzi, D. Izzo, and S. Theil, "Swarm Navigation and Reconfiguration using Electrostatic Forces," *7th International Conference on Dynamics and Control of Systems and Structures in Space*, Greenwich, London, England, July 2006, pp. 257–267.

[26] S. E. DeForest, "Spacecraft Charging at Synchronous Orbit," *Journal of Geophysical Research*, Vol. 77, Feb. 1972, pp. 651–659, doi:10.1029/JA077i004p00651.

[27] E. C. Whipple and R. C. Olsen, "Importance of differential charging for controlling both natural and induced vehicle potentials on ATS-5 and ATS-6," *Proceedings of the 3rd Spacecraft Charging Technology Conference*, Nov. 12–14 1980, p. 887. NASA Conference Publication 2182.

[28] H. Schaub and D. F. Moorer, "Geosynchronous Large Debris Reorbiter: Challenges and Prospects," *AAS Kyle T. Alfriend Astrodynamics Symposium*, Monterey, CA, May 17–19 2010. Paper No. AAS 10-311.

[29] P. Eremenko, O. Brown, and C. Roberts, "Cost-Benefit Analysis of a Notional Fractionated SATCOM Architecture," *24th AIAA International Communications Satellite Systems Conference (ICSSC) and 4th Annual International Satellite & Communications (ISCe) Conference and Expo*, San Diego, CA, June 11–14 2006. Paper No. AIAA-2006-5328.

[30] C. R. Seubert and H. Schaub, "Electrostatic Force Model for Terrestrial Experiments on the Coulomb Testbed," *61st International Astronautical Congress*, Prague, CZ, International Astronautical Federation, Sept. 2010. Paper IAC-10.C1.1.9.

[31] E. G. Mullen, M. S. Gussenhoven, D. A. Hardy, T. A. Aggson, and B. G. Ledley, "SCATHA Survey of High-Voltage Spacecraft Charging in Sunlight," *Journal of Geophysical Research*, Vol. 91, No. A2, 1986, pp. 1474–1490, doi:10.1029/JA091iA02p01474.

[32] J. F. Fennell, H. C. Koons, M. Leung, and P. Mizera, "A review of SCATHA satellite results: Charging and discharging," *1983.*, 1983, pp. 3–11.

[33] R. C. Olsen, "Modification of Spacecraft Potentials by Thermal Electron Emission on ATS-5," *AIAA Journal of Spacecraft and Rockets*, Vol. 18, Nov. – Dec. 1981, pp. 527 – 532.

[34] C. P. Escoubet, M. Fehringer, and M. Goldstein, "The Cluster Mission," *Annales Geophysicae*, Vol. 19, No. 10/12, 2001, pp. 1197–1200.

[35] K. Torkar, W. Riedler, and C. P. Escoubet, "Active Spacecraft Potential Control for Cluster – Implementation and First Results," *Annales Geophysicae*, Vol. 19, No. 10/12, 2001, pp. 1289–1302.

[36] W. R. Smythe, *Static and Dynamic Electricity*. McGraw–Hill, 3rd ed., 1968.

[37] J. Sliško and R. A. Brito-Orta, "On approximate formulas for the electrostatic force between two conducting spheres," *American Journal of Physics*, Vol. 66, No. 4, 1998, pp. 352–355.

[38] J. A. Soules, "Precise Calculation of the Electrostatic Force Between Charged Spheres Including Induction Effects," *American Journal of Physics*, Vol. 58, 1990, pp. 1195–1199.

[39] H. Schaub and J. L. Junkins, *Analytical Mechanics of Space Systems*. Reston, VA: AIAA Education Series, 2nd ed., October 2009.

[40] M. H. Denton, M. F. Thomsen, H. Korth, S. Lynch, J. C. Zhang, and M. W. Liemohn, "Bulk plasma properties at geosynchronous orbit," *Journal of Geophysical Research*, Vol. 110, 07 2005.

[41] N. Murdoch, D. Izzo, C. Bombardelli, I. Carnelli, A. Hilgers, and D. Rodgers, "The Electrostatic Tractor for Asteroid Deflection," *58th International Astronautical Congress*, 2008. Paper IAC-08-A3.I.5.

[42] R. H. Battin, *An Introduction to the Mathematics and Methods of Astrodynamics*. New York: AIAA Education Series, 1987.

[43] L. E. Z. Jasper and H. Schaub, "Effective Sphere Modeling for Electrostatic Forces on a Three-Dimensional Spacecraft Shape," *AAS/AIAA Spaceflight Mechanics Meeting*, Girdwood, Alaska, July 31 – August 4 2011.